Climatology of Mountain Venting–Induced Elevated Moisture Layers in the Lee of the Alps

STEPHAN HENNE, MARKUS FURGER, AND ANDRÉ S. H. PRÉVÔT

Laboratory of Atmospheric Chemistry, Paul Scherrer Institut, Villigen, Switzerland

(Manuscript received 27 June 2004, in final form 30 September 2004)

ABSTRACT

Elevated moisture layers in the lower free troposphere (2000–6000 m MSL) in the lee of the Alps were investigated. Specific humidity was analyzed within a Lagrangian concept for fair-weather days during a 12-yr period at the windward and the leeward sides of the Alps for the sounding sites of Payerne, Switzerland, and Milan, Italy. During daytime fair-weather conditions (different criteria), specific humidity increased significantly in air masses that advected from Payerne to Milan in a layer ranging from ~2500 to 4000 m MSL. The maximum relative increase of specific humidity in this layer was ~0.3, meaning that ~30% of the air in this layer originated from the Alpine atmospheric boundary layer. On average, ~30% of the mass of the Alpine boundary layer was vented to altitudes higher than 2500 m MSL per hour during the daytime. The total precipitable water within a layer reaching from 2500 to 3500 m MSL increased by ~1.3 mm. Similar elevated layers were observed for different selection methods of fair-weather days, and climatologically for the whole of June, July, and August. Average observations of the relative increase and boundary layer export rate agree with results from the local case studies. Daytime thermally driven flow systems seem to be the main source of additional water vapor in the observed elevated layers over the Alps. Subsequently, horizontal advection toward flat terrain where the average ABL top was well below the elevated layer bottom results in the export of ABL air to the free troposphere (mountain venting). Mountain venting was enhanced in situations with larger global radiation, lower atmospheric stability, and additional moist convection as was detected by lightning activity.

1. Introduction

Processes that lift air pollutants vertically from the ABL to higher altitudes range from synoptic to turbulent scales. Over flat terrain, mixing in frontal systems (synoptic scale), cloud convection, and turbulence (dynamically or thermally induced) are able to transport pollutants that are released at the earth's surface to higher altitudes. Over mountainous terrain vertical exchange is increased by enhanced dynamically induced turbulence, vertical motion in mountain waves (especially during wave breaking episodes), enhanced deep moist convection, and thermally driven flows (Kossmann et al. 1999).

High-altitude research stations [e.g., Jungfraujoch, Switzerland (JFJ) (Forrer et al. 2000), Mauna Loa, Hawaii (Mendonca 1969), and Colle Gnifetti, Italy (Lugauer et al. 1998)] are known to be influenced during daytime summer conditions by trace gases and aerosol [e.g., water vapor, carbon monoxide (Forrer et al. 2000), reactive nitrogen (Zellweger et al. 2000), aerosol surface area (Baltensperger et al. 1997)] originating from the ABL. It is suggested that vertical transport in a certain catchment area, rather than local slope winds, influences the concentrations that are measured at a mountain peak (Baltensperger et al. 1997; Seibert et al. 1998).

Airborne backscatter lidar measurements were used to characterize the development of the aerosol layer in the JFJ region (Nyeki et al. 2000). They observe an aerosol-layer top rising from about 2500 m MSL in the early morning to 4200 m MSL in the early afternoon. De Wekker et al. (2004) simulated the behavior of the aerosol layer for the same case study by means of numerical models and showed that the aerosol layer is not identical with the mixed layer, because the transport of aerosols to a certain altitude above the ABL occurred in the form of thermal injections rather than in a homogenous mixing process. The aerosol layer is slightly stable, nonturbulent in character, and capped by the stable free troposphere (FT) (De Wekker et al. 2004).

The same structure of atmospheric stability is found in an Alpine valley in southern Switzerland (Henne et al. 2004). It was shown that within the Alps slope, winds are an effective lifting mechanism carrying air pollutants up to ~4000 m MSL and causing high pollutant concentrations at crest height (Furger et al. 2000; Pre-

Corresponding author address: Dr. André S. H. Prévôt, Laboratory of Atmospheric Chemistry, Paul Scherrer Institut, 5232 Villigen, Switzerland.
E-mail: andre.prevot@psi.ch

vot et al. 2000). At this altitude synoptically influenced winds prevail, dispersing ABL pollutants over a larger domain. Mass export by thermally driven flow systems from two deep Alpine valleys within southern Switzerland was quantified for eight different cases by means of airmass budgets (Henne et al. 2004). Up to 3 times the valley's air mass is exported vertically per day.

Figure 1 depicts the idealized daytime flow structure of the thermally driven flow system within mountainous terrain. On fair-weather days, with strong global radiation and weak synoptic forcing, the thermally driven flow is directed into the mountains and upward (Whiteman 2000). Close to the surface a well-mixed ABL develops during the daytime. Within this layer specific humidity and air pollutants are well mixed in rural areas, as indicated by the vertical profile on the left-hand side of Fig. 1. Above the ABL, concentrations strongly decrease with height. Subsidence of air is expected on both sides of the mountains. Without any synoptic pressure gradients a closed circulation between the mountains and plains would result. The situation with an additional synoptic flow is shown in Fig. 1. Above the plain-to-mountain flow the wind is mostly synoptically driven. Air that is advected toward the mountains within the windward-side ABL is injected through gaps and steps in the ABL inversion (mountain venting) (Kossmann et al. 1999) into the synoptically influenced flow and is transported farther downwind.

An important question is whether vertically exported ABL pollutants and humidity are incorporated into the lower FT when they are advected toward the plains. If these elevated layers remain at higher altitudes than the ABL height of the adjacent plains, thermally driven flow systems would indirectly contribute to a net export of ABL pollutants to the FT. Downwind of the Alps over the Adriatic, elevated pollution layers are observed that are potentially related to the preceding vertical transport within the Alps (Nyeki et al. 2002).

In recent years the use of propagation delay of the global positioning system (GPS) signal enabled continuous observations of the total precipitable water (PW) column with high temporal resolution (~30 min), but without information on the vertical distribution (Rocken et al. 1995; Tregoning et al. 1998). Diurnal variations of PW with a maximum in the afternoon are observed over mountainous area of Sumatra Island (Wu et al. 2003) for days with strong solar radiation during the dry season (June–July–August). Above the broad valley (30-km width) of Lhasa at the Tibetan Plateau, a diurnal cycle of PW is observed that has its minimum in the afternoon (Takagi et al. 2000), indicating water vapor transport toward the surrounding mountains during the daytime. This is also supported by PW measurements above the mountains and numerical simulations (Kuwagata et al. 2001). In two different case studies during fair-weather conditions, moisture export from mountainous terrain to the Kanto Plain in Japan has been observed (Ohtani 2001; Iwasaki and Miki 2001). In the western Sumatra Mountains Sasaki et al. (2004) observed increased moisture in afternoon radio soundings in a layer up to 1000 m above the mixed layer for August 2001. Numerical simulations reproduce their findings and show that the ambient winds advect moist air over the plains.

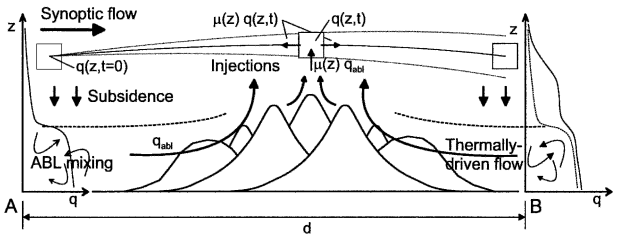

FIG. 1. Schematic of transalpine advection of an air parcel from the windward side station A to the leeside station B, during fair-weather, daytime conditions. See sections 1, 2b, and 2g for details.

Only case studies on moisture and airmass export due to mountain venting have been completed so far. To estimate the relevance of this process it is important to get climatological results for the occurrence and the strength of mountain venting. In our study a period of 12 yr is investigated. Elevated moisture layers in the Alpine region are detected by comparing soundings of specific humidity q at the windward and the lee side of the Alps. In section 2 we describe the applied methods and the datasets that were used. The concept of relative increase and ABL export rate is presented. In section 3 the results of the comparison in terms of profiles of specific humidity, PW, relative increase, and ABL export rate are presented. Dependencies of mountain venting on atmospheric parameters are analyzed. In section 4 we discuss the results and conclusions.

2. Methods

a. General concept and used datasets

The general idea of this investigation is to measure the composition of air parcels at different altitudes above the ABL in a Lagrangian concept before and after crossing the Alps. The windward sample A is considered as a background sample, showing smaller humidity and air pollutant concentrations than the ABL. Changes in the leeside sample B are then attributed to vertical lifting that transports pollutants and humidity upward over the mountainous terrain.

Water vapor is the only atmospheric constituent that originates from the earth's surface and is measured on climatological time scales throughout the whole troposphere. Therefore, observed changes in the vertical profiles of specific humidity in the windward and the leeward side of a mountainous region are the only adequate means to climatologically describe the lifting effect caused by thermally driven flow.

Two datasets were used in this study. Surface measurements of wind speed and direction, temperature, humidity, sunshine duration, global radiation, and lightning activity were taken from the automated MeteoSwiss (Swiss national weather service) surface station network (ANETZ). Measurements were used with a temporal resolution of 1 h for the period from January 1991 to December 2002. A total of 72 surface stations were available within this dataset with an altitude range from 197 to 3580 m MSL. The second dataset of upper-air measurements of wind speed and direction, temperature, pressure and humidity included two sounding sites, Payerne, Switzerland (46.82°N, 6.95°E; 491 m MSL), situated on the Swiss plateau north of the Alps, and Milan, Italy, within the Po basin (45.43°N, 9.28°E; 102 m MSL) south of the Alps (Fig. 2). The data were taken from the quality-checked Comprehensive Alpine Radiosonde Data Set (CALRAS) (Haberli 2002) database. At Payerne two radio soundings per day [0000 and 1200 UTC (LT = UTC + 1)] for temperature, pressure, and humidity, and four soundings per day (0000, 0600, 1200, and 1800 UTC) for wind speed and direction, were available for the period from January 1991 to December 2002. At Milan four radio soundings per day (0000, 0600, 1200, and 1800 UTC) for temperature, pressure, humidity, and wind speed and direction were available for the same period.

The analysis was done for fair-weather days within a 12-yr period to derive a climatological estimation of mountain venting over the Alps. Different criteria to select fair-weather days are described in section 2f.

The vector-averaged wind speed ff and direction dd for a 12-h period were calculated at every altitude from all of the available soundings during this period and from both sounding stations. This usually resulted in six considered soundings.

b. Cross-Alpine flow on fair-weather days

On fair-weather days an air parcel that travels from point A to B across the mountains with the synoptically driven wind is influenced by vertical transport in the form of thermal injections over the mountains (Fig. 1). When the air parcel arrives at point B in the lee of the mountains its composition (e.g., specific humidity) might be modified (vertical profile on right side, windward profile indicated by a solid line, modified profile indicated by a dotted line). Fair-weather days are usually connected with subsiding air within high pressure systems. Over mountainous terrain this subsidence is counteracted by upward motion within the mountain heat low. Therefore, the altitude of a certain air parcel advected across the mountain is not expected to be altered considerably from the windward to the lee side (see section 3c for further discussion).

In our case points A and B are represented by Payerne and Milan, respectively. The distance between both stations is 237 km. An air parcel would need to travel with an average speed of 5.5 m s^{-1} to start from one station and arrive at the other within 12 h. If we consider an individual sounding being representative for ±50 km along the wind direction, average traveling speeds between 4.4 and 6.6 m s^{-1} would be adequate to fit into the Lagrangian concept.

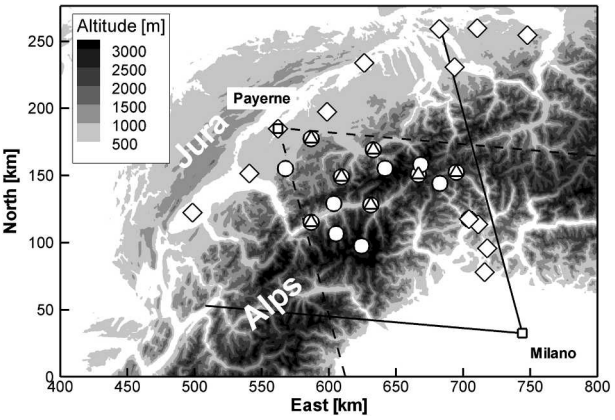

FIG. 2. Overview of measurement sites and Alpine terrain: radio sounding stations (squares); stations used for global radiation and sunshine duration measurements (diamonds); surface stations for inner Alpine boundary layer measurements (deltas); and lightning, rain, and solar radiation measurements for evapotranspiration calculation (circles). Overlay of symbols indicates double use. The catchment area of the Milan soundings is indicated by the thick solid line (thick dashed line for Payerne). Horizontal coordinates are given in the Swiss coordinate system.

Figure 3 shows the median terrain height in a 50-km strip connecting Payerne and Milan. The median terrain height is about 2500 m MSL in the central Alpine region, with up to 25% of the surface being higher than 3000 m MSL. The upper *x* axis provides the time for an air parcel that travels with 5.5 m s^{-1} arriving in Milan at 0000 UTC. Because thermally driven flow lasts at least until 1700 UTC and all terrain above 1500 m MSL might contribute to the lifting processes, the air parcel might receive injections of ABL air between 1330 and 1700 UTC. For altitudes lower than 2500 m MSL the

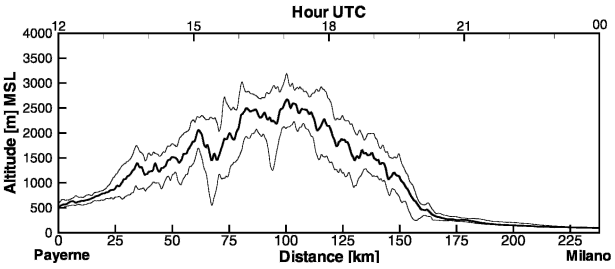

FIG. 3. Terrain height between Payerne (0 km) and Milan (237 km). Thick solid line represents median height of a 50-km-wide strip between both stations, thin solid lines correspond to lower and upper quartile. Note that vertical dimension is amplified. The upper *x* axis gives the time for an air parcel arriving from Payerne at Milan at 0000 UTC, traveling with an average wind speed of 5.5 m s^{-1}.

results should not be interpreted in a Lagrangian perspective, because direct flow could be blocked by the mountain barrier.

c. Excluded situations

To ensure that vertical transport is not dominated by processes other than thermally driven flow systems, different criteria were used to exclude these situations to the greatest possible extent.

Large wind speeds, in combination with a stably stratified atmosphere, are able to force gravity waves (mountain waves), followed by possible wave breaking and, hence, vertical mixing (Durran 1990). Therefore, cases with ff larger than 10 m s^{-1} at any investigated altitude were excluded from the study.

Vertical exchange processes previous to the "background" sounding A might result in elevated moisture layers at A. These layers might mask the process of further vertical exchange when upper-air concentrations were already as large as in the ABL. Soundings that showed a secondary maximum in specific humidity in the "background" sounding at an altitude higher than 2000 MSL with a thickness of at least 500 m were excluded from the analysis.

Investigated days were divided into days with and without deep moist convection by using close-range (distance <5 km)-recorded lightning activity from the Swiss ANETZ surface station network. Days that showed lightning activity during the investigated transalpine transport at any ANETZ station between Payerne and Milan (circles in Fig. 2) were summarized as "lightning" cases, and days without lightning were "no lightning" cases.

Days with more than 1-mm precipitation during the investigated transalpine transport at any of the same stations were excluded from the no-lightning cases. If precipitation occurred in combination with lightning the case was still investigated in the lightning category.

The exclusion criteria are summarized in Table 1.

TABLE 1. Excluded situations for lightning and no-lightning category. See section 2b for details.

Subcategory	Wind speed	Elevated layer at A	Precipitation
No lightning	>10 m s^{-1} excluded	Excluded	>1 mm excluded
Lightning	>10 m s^{-1} excluded	Excluded	All included

d. Evapotranspiration

An additional source of humidity in the leeside soundings at B might result from surface evapotranspiration from elevated terrain during the transalpine transport. Evapotranspiration ET (mm h^{-1}) for an air parcel crossing the Alps was estimated by applying an empirical formula that needs solar radiation R_s, temperature T, and relative humidity RH as input parameters, and was actually developed for adequately watered crop fields (Alexandris and Kerkides 2003):

$$\mathrm{ET} = \mathrm{ET}(R_s, T, \mathrm{RH}). \quad (1)$$

For every investigated category (see section 2f) these input parameters were calculated on an hourly basis for every investigated altitude. Incoming solar radiation was assumed to be rather constant with height and was taken from ANETZ stations between Payerne and Milan (circles in Fig. 2). Initial vertical profiles of temperature and relative humidity were taken from the average windward radio soundings. Evapotranspiration derived by (1) was assumed to be dispersed homogeneously within a vertical layer $\Delta z = 100$ m. The hourly ($\Delta t = 1$ h) increase of specific humidity Δq (g kg^{-1}) was derived by

$$\Delta q = \frac{\mathrm{ET} f_a \Delta t \rho_{\mathrm{H_2O}}}{\Delta z \rho}, \quad (2)$$

where f_a is the surface fraction at every investigated altitude, $\rho_{\mathrm{H_2O}}$ is the density of liquid water, and ρ is the air density at every investigated altitude. Surface fractions were calculated using a 250 m × 250 m digitized topography model. This calculation also accounted for nonhorizontal surfaces, so that the sum of all surface fractions was larger than 1. Evapotranspiration was iteratively calculated for 12 h. Because the mountainous terrain above 2000 m is covered to a large percentage by rocks, we assume that the calculated evapotranspiration is an overestimation of the real value.

e. Averaging method

Two different approaches were designed to investigate the average differences between the windward and leeside soundings; the first took separate layers into account (layer method hereinafter), and the second used the entire vertical profiles (profile method). For both methods the sampled profiles were divided into equidistant layers with a vertical extension of 100 m. The layer method analyzed the vector mean wind direction dd (see section 2a) at every individual altitude. If dd was within ±35° from the connecting line between stations A and B, the case was added to the averaging process. This was done for all selected days. The catchment sectors for Milan and Payerne can be seen in Fig. 2. The selected wind range implies that the windward sounding is representative for ±160 km on a circular arc through the windward station, which is reasonable for advection from Payerne to Milan because of the terrain-height homogeneity in this direction.

In contrast to the layer method, the profile method used the whole profile of an individual day. If the vector mean of dd within the layer between 2000 and 5000 m MSL matched the connection line between stations A and B by ±35°, the whole profile was added to the average profile.

f. Categories to select fair-weather days

To investigate the effect of thermally driven flow systems on the leeside profiles of specific humidity, five different selection criteria for fair-weather days were used.

The first two criteria used data that were taken from the surface station network. Stations on both sides of the Alps—representative for the northern (10 stations) and southern (4 stations) Alpine forelands (diamonds in Fig. 2)—were selected. These stations covered the whole Swiss plateau in the west–east direction and the Ticino area south of the Alps. On fair-weather days it is very likely that cumulus clouds develop in the Alps. These might very locally change the amount of incoming solar radiation at the surface. Therefore, only stations outside of the Alps were selected. To avoid local influence, radiation data were used from more than one individual station.

If the total sunshine duration per day ΣS was larger than 9 h for at least 50% of the stations in the north and 50% of the stations in the south, a day was categorized as being a "sun day" (SND). A similar criterion is used to investigate thermally driven flow in the Bavarian forelands in southern Germany (Lugauer and Winkler 2005).

If the total amount of incoming solar radiation per day to the earth's surface ΣR_s was larger than 19 MJ m^{-2} at more than 50% of the stations in the north and south, a day was categorized as being a "radiation day" (RAD).

The other three categories used parameter 33 of the Alpine Weather Statistics (AWS) (Schuepp 1979; Wanner et al. 1998). The so-called Schüepp classification system contains 40 weather situations for the western Alpine region. For our analysis we selected days within the main category ("convective") that compromises days with weak horizontal wind speeds at 500 hPa. The convective category is further divided into the following categories: "anticyclonic" (ANT), "indifferent" (IND), and "cyclonic" (CYC). To focus on days with a large potential for thermally driven flow, the selection was further confined to the months of March–September.

Figure 4 shows the average number of selected days per month for the 12-yr period. In addition, the number of selected days and the average values for ΣR_s, ΣS are summarized in Table 2. For the SND and RAD categories the selected days were mostly limited to the months from March to September, with a maximum in July and August. About 60% of all summer days fulfilled the RAD criterion. The number of days within the IND category was larger within the summer months, whereas the categories ANT and CYC showed no general dependence on the season. The average ΣR_s was largest for the days selected by the SND and RAD criteria, and was slightly lower for the ANT and IND categories, while it was much lower for the CYC category. Sunshine duration ΣS was largest for the days chosen by the SND criterion, followed by the ANT, RAD, and IND categories. Here, ΣS was much shorter for the CYC category.

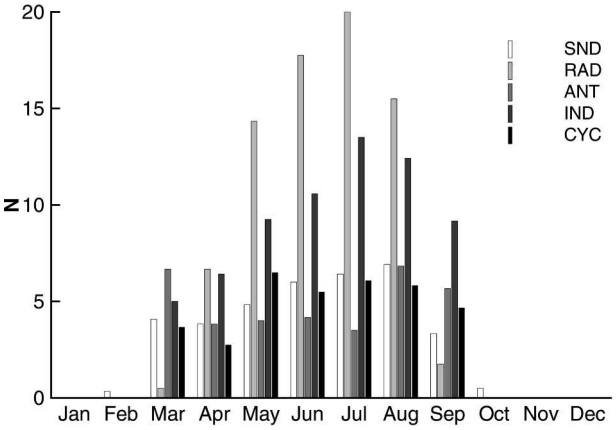

FIG. 4. Average monthly distribution of days selected by the SND, RAD, ANT, IND, and CYC categories.

In addition to these categories based on the current weather situation, days were categorized by season (SEA). Table 2 shows that ΣR_s and ΣS for the summer months [June–July–August (JJA)] compare to the IND category.

Further on, the categories were subdivided into a no-lightning and lightning category (see section 2c), indicated with the subscripts "nl" and "l," respectively, as follows.

g. Relative increase and ABL export rate

For pollutant budget calculations it is important to quantify the export of ABL air to the FT. By knowing the specific humidity at the windward side of the mountains q_a, in the lee of the mountains q_b, and within the mountainous ABL q_{abl}, it is possible to calculate the relative increase (ri) (Prevot et al. 2000) in specific humidity at a certain altitude z above the ABL:

$$\mathrm{ri}(z) = \frac{q_b(z) - q_a(z)}{q_{\mathrm{abl}} - q_a(z)}. \tag{3}$$

TABLE 2. Investigated categories. See section 2f for details.

Category	Selection	N	ΣS (h)	ΣR_s (MJ m^{-2})
SND	Total sunshine duration >9 h day^{-1}	540	11.3	23.1
RAD	Total global radiation >19 MJ m^{-2} day^{-1}	918	10.0	22.9
ANT	Anticyclonic weather type (Mar–Sep)	416	10.3	20.7
IND	Indifferent weather type (Mar–Sep)	769	7.1	18.2
CYC	Cyclonic weather type (Mar–Sep)	420	3.1	11.3
JJA	Summer season	1104	7.55	19.0

Here, q_{abl} was taken as the average specific humidity during the thermally driven flow (0900–1700 UTC) at the surface stations (indicated with deltas in Fig. 2). These stations are all situated within the Alps at different altitudes between 580 and 1350 m MSL. The station-to-station variability was lowest for this selection. Including the stations at higher altitudes (<2000 m MSL) strongly increased the variability; ri varied about ±8% when including different numbers of ABL stations. Therefore, we think our selection is representative of the Alpine ABL. The calculation of ri, which gives the percentage of ABL air that was transported to a certain altitude, was done for every individual day.

Further, it was possible to estimate the fraction of air that leaves the ABL per hour. For this purpose the residence time t_r of an air parcel over mountainous terrain during active thermally driven flow was calculated for individual days. Thermally driven flow was assumed to persist from 0900 to 1700 UTC. Average wind speed and direction ff and dd (see section 2a) were used to calculate the residence period over mountainous terrain (a median altitude larger than 1500 m MSL) of an air parcel arriving at B for every investigated altitude. The intersection of both periods resulted in t_r.

We considered an air parcel with constant volume that receives injections of ABL air at a constant mass flux density μ with the concentration q_{abl} (Fig. 1). These injections can be regarded as thermal plumes that start within the ABL and reach certain altitudes; further vertical exchange between different elevated altitudes is not considered in this simplified model. At the same time because of continuity the same flux leaves the air parcel horizontally with the concentration $q(t)$. The change of q with time is then given by

$$\frac{\partial q(z)}{\partial t} = \frac{\mu(z)}{\rho(z)}[q_{\mathrm{abl}} - q(z, t)]. \tag{4}$$

The concentration at time $t = 0$ was given by the sounding at A, $q(t = 0) = q_a$. Solving the differential equation (4) for $q(t)$ yields

$$q(z, t) = q_{\mathrm{abl}} + [q_a(z) - q_{\mathrm{abl}}] \exp\left[- \frac{\mu(z)}{\rho(z)} t \right]. \tag{5}$$

Here, μ can be written in terms of the fraction f_e of the ABL mass per surface area $\rho_{\mathrm{abl}} h_{\mathrm{abl}}$ that is vented from the ABL to a certain height per unit time

$$\mu(z) = f_e(z) \rho_{\mathrm{abl}} h_{\mathrm{abl}} f_v, \tag{6}$$

where f_v is the volume correction factor that considers the reduced volume of the ABL due to elevated terrain. We will refer to f_e as the ABL export rate hereinafter. Because calculations are done with a vertical resolution of $\Delta z = 100$ m, values for the ABL export rate $(\mathrm{s\ m})^{-1}$ will be given as $f_e\, \Delta z$ (h^{-1}). Inserting q_b for $t = t_r$ and (6) in (5) and solving for f_e yield

$$f_e(z) = \frac{\ln\left[\dfrac{q_{\mathrm{abl}} - q_b(z)}{q_{\mathrm{abl}} - q_a(z)} \right] \rho(z)}{\rho_{\mathrm{abl}} h_{\mathrm{abl}} f_v t_r(z)}. \tag{7}$$

Here, h_{abl} was calculated as an average of both 1200 UTC soundings (Payerne and Milan) with a simple parcel method that assumes h_{abl} to be the altitude where the temperature of a parcel with the initial surface temperature that is lifted dry adiabatically from the surface intersects with the temperature of the current sounding. Under strong irradiation, but otherwise stable conditions, this method is in good agreement with more complex methods of determining h_{abl} (Seibert et al. 2000). Here, $\rho(z)$ was taken from the soundings, ρ_{abl} was taken as the average ρ for altitudes lower h_{abl}, f_v was calculated using topographic information in a 250 m × 250 m grid of a strip of a 50-km width connecting Payerne and Milan, and f_e was calculated for every altitude each day. The total fraction of ABL air that is exported per unit time (s^{-1}) f_t was derived by the integration of f_e for the altitude range 2500–6000 m MSL,

$$f_t(z) = \int_{z'=2500}^{z'=6000} f_e(z')\, dz. \tag{8}$$

The lower limit of this altitude range was chosen because it remained unclear if the method is applicable underneath. An estimation of h_{abl} was made over the forelands. It is not straightforward to determine the actual ABL height within the Alps. It is likely that the ABL is higher in the Alps than over flat terrain. Therefore, f_e presents an upper limit of the export rate. On the other hand, the integration of f_e to derive f_t does not account for altitudes lower than 2500 m MSL. Therefore, f_t might be underestimated. Because the possible errors have opposite signs, the calculation of f_t should be reasonable.

Because fewer assumptions are necessary to calculate ri as compared with f_t, the analysis of ri is more robust. On the other hand f_e and f_t should be independent from the synoptic wind speed and, therefore, offer a more general conclusion.

3. Results

a. Payerne–Milan

Figure 5 shows vertical profiles of q as calculated by the layer method for the soundings at Payerne at 1200 UTC and Milan at 0000 UTC of the following day for the SND category, with no lightning ($\mathrm{SND_{nl}}$) (wind direction from Payerne toward Milan). Average specific humidity decreased from 1000 to 2500 m MSL for Payerne at 1200 UTC (thick solid line); farther up the decrease lessened. Up to 4100 m MSL the average specific humidity was larger in the 0000 UTC Milan profile (thick dashed line) in comparison with the 1200 UTC Payerne profile, above which the differences were

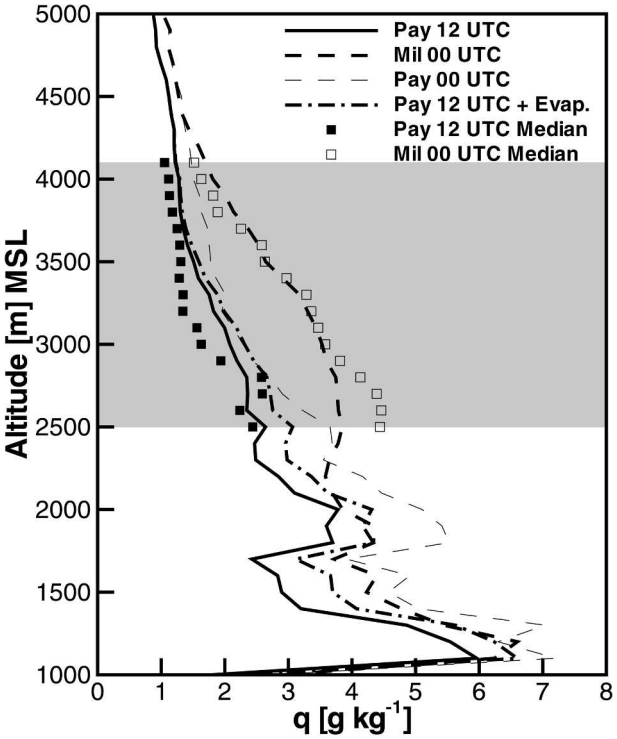

FIG. 5. Vertical profiles of specific humidity q for SND no-lightning cases, as measured in Payerne at 1200 UTC [average (thick solid line), median at significant levels (solid squares)], in Milan at 0000 UTC [average (thick dashed line), median at significant levels (open squares)], and in Payerne at 0000 UTC [mean (thin dashed line)]. The gray area indicates the elevated layer. In addition, evapotranspiration was calculated for a 12-h period and added to the average 1200 UTC Payerne measurements (thick dashed–dotted line).

small. In addition to the average profiles, median values are given for altitudes that show a significant difference between both stations [we used a Mann–Whitney test (Mann and Whitney 1947) and stated a significant difference if the probability of error was lower than 0.01, and at least 25 samples were included at a certain altitude]. The median profiles and the average profiles were similar. A layer ranging from 2400 to 4100 m MSL showed significant increases in q, which almost doubled in this layer. We will refer to such layers as "elevated layers" in the following and assume that they show a significant difference to the windward sounding, if not stated otherwise. In addition, the average profile for the 0000 UTC Payerne soundings is shown in Fig. 5 (thin dashed line). Throughout the whole lower troposphere, and especially at about 2000 m MSL, q increased, but the general structure of the profile did not change relative to the 1200 UTC Payerne profile. This increase might be related to synoptic-scale advection or larger-scale vertical motions due to atmospheric tides (Dai et al. 2002; Whiteman and Bian 1996), or vertical mixing over flat terrain or the Jura Mountains that are northwest of Payerne (see Fig. 2).

Estimated water vapor due to evapotranspiration during the 12-h transport time from Payerne to Milan accounted only for a small increase throughout the lower troposphere (thick dashed–dotted line). Only below 2200 m MSL evapotranspiration might explain the increase in specific humidity from Payerne to Milan. But, as mentioned above, the Lagrangian perspective might not be reasonable within this altitude range. As mentioned before, evapotranspiration was most likely overestimated. This fact further minimizes the impact of evapotranspiration as an additional water vapor source during advection. Therefore, all further comparisons focus on the differences between the original soundings at A and B, neglecting the estimated evapotranspiration.

Figure 6 gives the number of cases N that were used in the averaging and the average wind speed ff at every altitude for the SND_{nl} category. Direct flow from Payerne toward Milan was less frequent below 2500 m MSL. A broad maximum in frequency at about 4000 m MSL with up to 80 cases was observed. At higher altitudes the average wind speed was often too high to suit the selection criterion. The gray area in Fig. 6 marks the wind speed range from 4.4 to 6.6 m s^{-1}, which is favor-

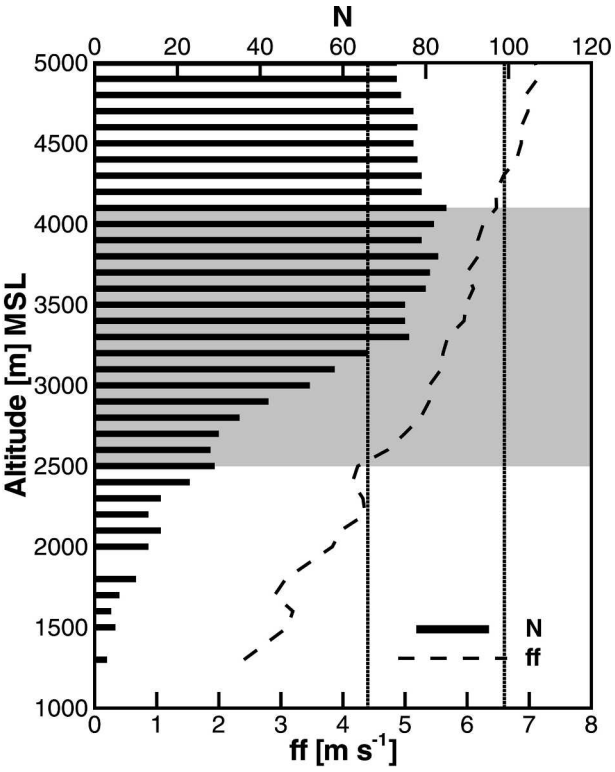

FIG. 6. Vertical profiles of average wind speed ff for the same category as in Fig. 5. The gray area indicates the elevated layer, and the area between the two vertical lines shows the wind speed range that is suitable for the Lagrangian concept. The number of included cases for the averaging at each altitude is displayed by the horizontal bars.

able for the Lagrangian concept (see section 2b). Between 2500 and 4300 m MSL the wind speed lay within this range.

The results for the RAD_{nl} category were very similar to the SND_{nl} category. Figure 7 shows vertical profiles of specific humidity for the RAD_l category (the SND_l category is not shown because of the small number of cases in this category). Again, a strong increase in specific humidity was observed from Payerne at 1200 UTC to Milan at 0000 UTC. However, the "elevated layer" reached higher, up to 4800 m MSL, relative to the case without lightning. Even if the increase in specific humidity was large below 3200 m MSL, it was not considered to be significant because less than 25 cases were available at these altitudes. The observations suggest that thermally driven flow and moist convection act together in producing the resulting profile in Milan at 0000 UTC. Because moist convection is incorporated with cloud condensation and possible precipitation it remains unclear if specific humidity can be used as a conservative quantity in the context of thunderstorm activity.

Figure 8 shows the vertical profile of the relative increase ri (dashed line) and the ABL export rate f_e for the SND_{nl} category. Below 2400 m MSL a large scatter in ri was observed for individual samples and ri showed large values that should not be interpreted. A maximal ri value was reached within the elevated layer at ~2700 m MSL of 0.3, meaning that 30% of the air in this layer originated from the ABL. Up to 3400 m MSL ri was larger than 0.2, and above 4000 m MSL ri decreased to values of about 0.01. The air between 2400 and 3800 m MSL, thus, contained more than 20% air that originated from the Alpine ABL. In addition to ri the vertical profile of the export rate f_e for the ABL between Payerne and Milan is shown. Because f_e incorporates the transport time, profiles of ri and f_e differ in shape. The lower wind speeds at lower altitudes tended to increase ri. Between 2400 and 3500 m MSL, f_e was rather constant for the significant layer (about 0.017 h^{-1}), meaning that the mass flux to this layer was relatively independent of height. Above 4000 m MSL f_e decreased to values lower than 0.004 h^{-1}. Integrating f_e for the altitude range of 2500–6000 m MSL yielded a total fractional ABL air export rate f_t of 0.31 h^{-1}. This means that about 31% of the Alpine boundary layer was injected per hour to altitudes above 2500 m MSL.

Table 3 summarizes the results on elevated specific humidity layers for different categories of days. The results for the selection SND_{nl} and RAD_l have already been discussed. For RAD_{nl} the characteristics of the elevated layer were similar to SND_{nl}, showing that the sunshine criterion can be relaxed to the radiation criterion, without loosing the general pattern in the results. RAD_{nl} includes 133 cases, instead of 85 for SND_{nl}. The maximal observed ri within the elevated

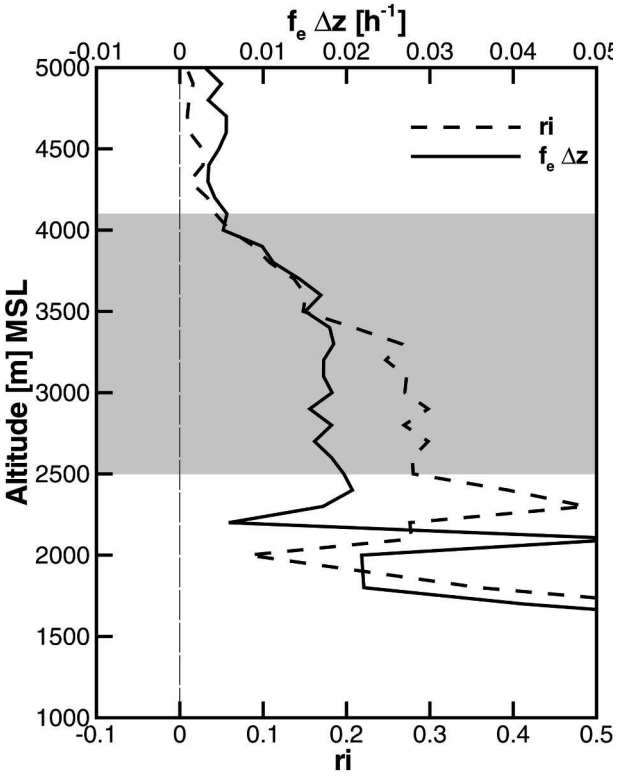

FIG. 8. Relative increase in specific humidity ri (dashed line) and ABL export rate $f_e \Delta z$ (thick line) for the SND no-lightning cases for Payerne at 1200 UTC and Milan at 0000 UTC. The gray area indicates the elevated layer (see Fig. 5).

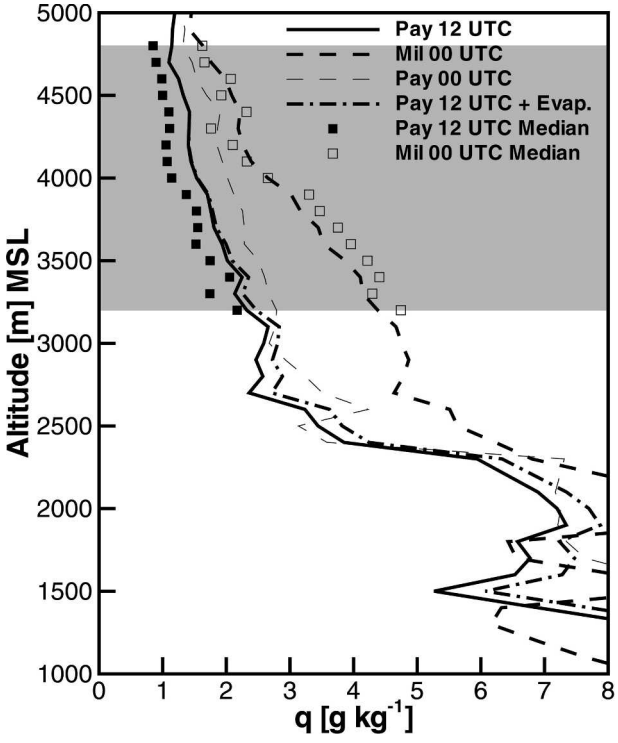

FIG. 7. Same as Fig. 5, but for RAD lightning cases.

TABLE 3. Summary of elevated-layer characteristics and PW differences for advection from Payerne toward Milan and different categories.

	Selection	Lightning	Range[a] (km) MSL	ri_{max}[b]	Δq_{max}[c] (g kg^{-1})	N_{max}[d]	f_t[e] (h^{-1})	ΔPW_{il}[f] (mm)	$\Delta PW_{il,e}$[g] (mm)	$\Delta PW_{il,l}$[h] (mm)	h_{abl}[i] (km) MSL
	SND_{nl}	No	2.4–4.1	0.30	1.5	85	0.31	1.36	0.23	0.38	1.2
	SND_{l}	Yes	—	—	—	—	0.23	2.14	0.24	0.33	1.2
	RAD_{nl}	No	2.5–4.2	0.27	1.5	133	0.30	1.24	0.20	0.31	1.3
	RAD_{l}	Yes	3.2–4.8	0.41	2.1	44	0.30	2.09	0.22	0.56	1.3
	ANT_{nl}	No	2.7–3.9	0.27	1.7	61	0.32	1.45	0.23	0.30	1.1
	IND_{nl}	No	2.9–4.1	0.24	1.3	80	0.25	0.87	0.16	0.41	1.2
	CYC_{nl}	No	—	—	—	—	0.19	0.25	0.10	0.22	1.3
	MAM_{nl}	No	—	—	—	—	0.14	0.25	0.16	0.11	1.2
SEA	JJA_{nl}	No	2.6–4.2	0.33	1.7	122	0.32	1.21	0.17	0.36	1.3
	SON_{nl}	No	—	—	—	—	−0.02	−0.10	0.09	0.04	0.9
	DJF_{nl}	No	—	—	—	—	−0.17	−0.40	0.08	−0.05	0.8

[a] Extent of layer showing significant differences in specific humidity.
[b] Maximum relative increase of q within elevated layer.
[c] Maximum absolute increase of q within elevated layer.
[d] Maximum number of days investigated within elevated layer.
[e] Total ABL export rate.
[f] Difference in precipitable water within IL between windward- and leeside soundings.
[g] Difference in precipitable water within IL due to evapotranspiration.
[h] Difference in precipitable water within IL between 1200 and 0000 UTC windward soundings.
[i] Average ABL height over surroundings.

layer was somewhat higher in the SND_{nl} than in the RAD_{nl} selection, 0.30 and 0.27, respectively. Both selections showed a similar maximal increase in specific humidity Δq_{max} of 1.5 g kg^{-1}. For SND_l the significance of the elevated layer could not be assessed.

For all other selections only the cases without lightning are discussed. On ANT_{nl} an elevated layer was observed in the leeside sounding in the range from 2700 to 3900 m MSL. The characteristics of this layer were similar to the categories RAD_{nl} and SND_{nl}. Within IND_{nl}, a narrower elevated layer was observed, reaching from 2900 to 4100 m MSL and showing smaller values for ri and Δq than the previous categories. For CYC_{nl}, no significant increase was observed. The seasonal analysis revealed a broad elevated layer (2600–4200 m MSL) for the JJA_{nl} period, with a maximal ri of 0.33 and Δq of 1.7 g kg^{-1}. For the no-lightning March–April–May (MAM_{nl}), no-lightning September–October–November (SON_{nl}), and no-lightning December–January–February (DJF_{nl}) seasons, no elevated layers were observed. Because radiative input was already large in MAM, we expected to observe an elevated layer for this time period. But the larger snow cover in the Alps in MAM might have caused a larger albedo. Therefore, less sensible heat was available to heat the atmospheric surface layer and the development of thermally driven flow systems might have been reduced. On the other hand, atmospheric stability is lower in spring because the upper atmosphere is still relatively cool. This results in enhanced cloud formation, thunderstorms, and, therefore, reduced incoming global radiation.

The total ABL export rate f_t was similar for the SND_{nl}, RAD_{nl}, ANT_{nl}, and JJA_{nl} selection (Table 3). The IND_{nl} category showed a somewhat lower value. It is interesting to note that also for selections that did not show an elevated layer, f_t was positive. For the MAM_{nl} season f_t was 0.14 h^{-1}, showing that vertical export could already be strong in spring, even if the increase in specific humidity was not significant for the whole period. Further analysis of the individual months showed that elevated layers were present for the months of May–August but not for March, April, or September.

In addition to the layer characteristics, PW was calculated from the average q profiles (together with average profiles of temperature and atmospheric pressure). Differences from the background profile are presented for the altitude range from 2500 to 3500 m MSL [injection layer (IL, subscript il) here following] (Table 3). This altitude range was chosen because the largest absolute changes in specific humidity were observed within this range. The difference between the 0000 UTC Milan and 1200 UTC Payerne soundings is ΔPW_{il}. In this context, the subscript "e" refers to the increase due to evapotranspiration, and the subscript "l" refers to the local change and was calculated from the 1200 and the following 0000 UTC Payerne profiles. For all of the selections that show elevated layers, the largest change in PW was observed between the 0000 UTC Milan and the 1200 UTC Payerne soundings, with ΔPW_{il} being as large as 1.4 mm. The change due to evapotranspiration $\Delta PW_{il,e}$ was 1/5–1/7 the size. Because evapotranspiration was rather overestimated, it can be regarded as a minor additional source of humidity at elevated levels. The local change $\Delta PW_{il,l}$ was 1/3–1/4 times ΔPW_{il}. The local change itself might be influenced by vertical mixing over the Jura Mountains upstream of Payerne.

For selections including lightning ΔPW_{il} was even larger (~2 mm). The cyclonic weather type showed a

small increase in ΔPW_{il} that was similar to the local change, indicating that this change was rather synoptically influenced than being due to thermally driven flow. Within the MAM_{nl} season PW_{il} increased as much as 0.25 mm from Payerne to Milan, which was about twice as much as the local change, but less than the local change and the change due to evapotranspiration together.

From Payerne to Milan PW_{il} decreased during SON, and especially during the DJF_{nl} season, while the local change was rather small. Because days with rain were excluded from the study it is likely that subsidence dominated the lower layers of the Alpine atmosphere during the cold season and was responsible for this decrease.

The average ABL height at Payerne and Milan was much lower than the lower limit of any observed elevated layer for all investigated categories (see Table 3). By leaving the Alpine region these elevated layers, therefore, became part of the lower FT.

Figure 9 shows profiles of q for nighttime advection from Payerne at 0000 UTC to Milan at 1200 UTC for the SND_{nl} category. During this period a horizontally advected air parcel is not expected to be influenced by daytime thermally driven flow, which starts after the air parcel leaves the Alps (cf. Fig. 3). In contrast to increasing q during the daytime and the predicted slight increase due to evapotranspiration (dashed–dotted line), q decreased at the lee side throughout the whole lower troposphere, relative to the windward side. This might be related to a large-scale subsidence in high pressure systems dominating the sample. Especially below 2500 m MSL q strongly decreased in the leeside soundings. The decrease in q at Payerne itself was about the same as in Milan at 1200 UTC.

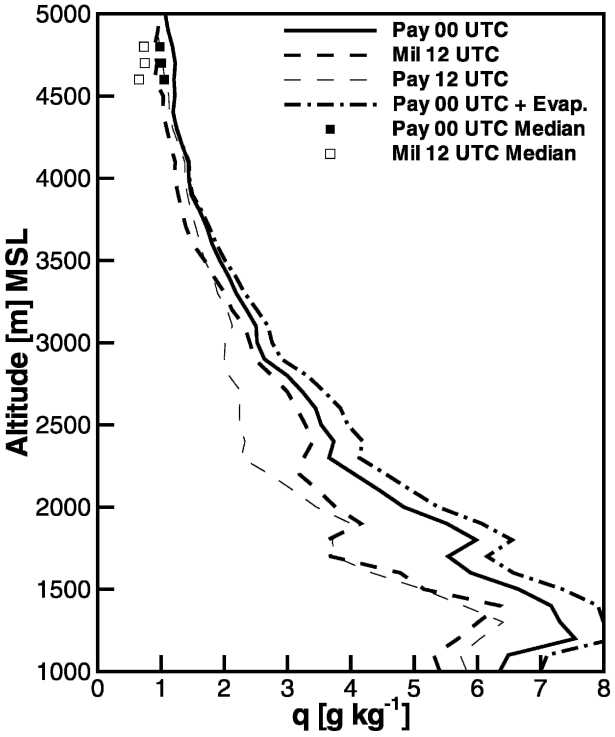

FIG. 9. Same as Fig. 5, but for nighttime advection.

b. Milan–Payerne

For advection from Milan toward Payerne in the range of 2500–4000 m MSL only 9 days out of the 12-yr period met the SND_{nl} criterion (7 days for RAD_{nl}). A weather situation with advection from the southeast is rather infrequent for the Alpine region. The average specific humidity increased only slightly from Milan at 1200 UTC to Payerne at 0000 UTC for the SND_{nl} case. In addition, the 0000 UTC Milan soundings showed the same change as the 0000 UTC Payerne soundings. The same resulted for the RAD case with lightning and the AND, IND, and JJA cases with or without lightning.

Of all selected days with advection from Milan toward Payerne in the range of 2500–4000 m MSL only 1 day lay within the summer month—8 July 1995. All of the other days were within the spring or autumn season. Only for the case in July was a well-defined increase in specific humidity in the lee sample observed.

Specific humidity was generally larger up to 5000 m MSL in the leeside sounding in Payerne at 0000 UTC than in Milan at 1200 UTC. The windward sounding at 0000 UTC showed uniform specific humidity up to 1800 m MSL and a strong decrease above with generally lower values than on the lee side. In the IL PW increased by 2.8 mm from Milan to Payerne, while locally PW decreased in the IL by 0.1 mm at Milan.

This case underlines that elevated layers in the lee of the Alps are also formed during southeasterly advection. Unfortunately, statistical proof was not possible because of the rare occurrence of this situation.

c. Further considerations of the method

The layer method does not represent a real average over complete profiles, but only an average at every height level. Figure 10 presents the results for the profile method for the SND no-lightning case. Despite the fact that the profiles are somewhat smoothed in comparison with Fig. 5, no general difference between both methods was observed within the elevated layer that resulted from the layer method (2500–4100 m MSL). Below 2500 m MSL q increased more and was generally larger using the profile method than using the layer method. This might result from situations with wind shear in the lower troposphere and southern advection in the ABL at Milan and southwesterly advection at Payerne. These situations would contribute to the average of the profile method but not to the layer method.

Average potential temperatures θ (Fig. 11) increased during the daytime transport from Payerne to Milan by about 2 K in the elevated layer (SND, RAD, ANT, and

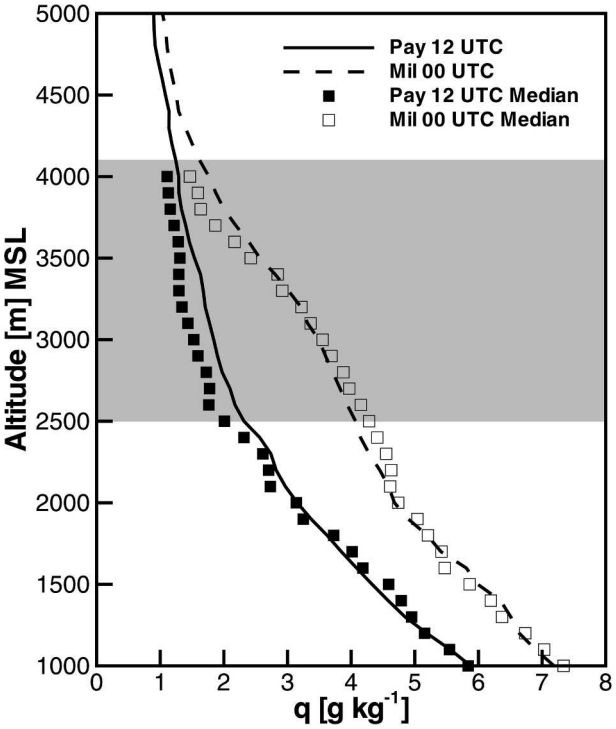

FIG. 10. Same as Fig. 5, but estimated with profile method. The gray area indicates the elevated layer as observed by the layer method (see Fig. 5).

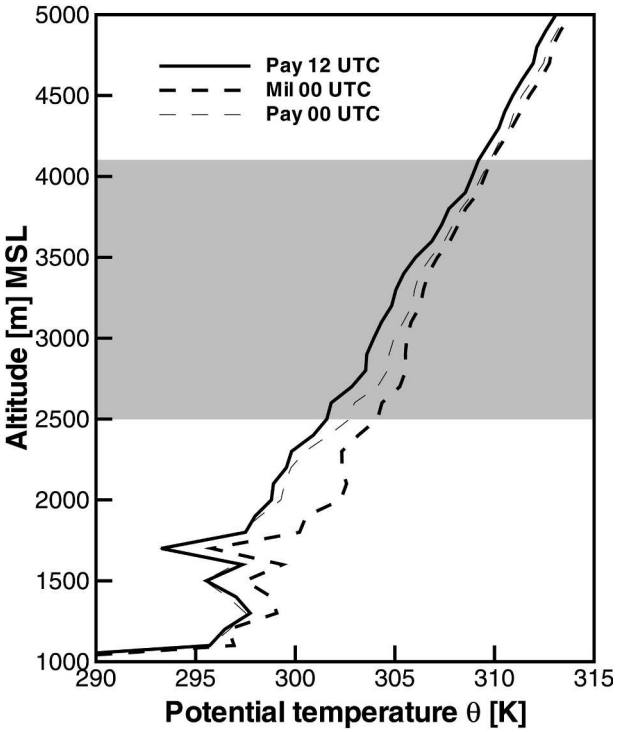

FIG. 11. Vertical profiles of potential temperature θ for the same selection as in Fig. 5. The gray area indicates the elevated layer.

IND categories). Because mixing and diabatic processes might be active in this altitude range, it was not possible to attribute the warming to adiabatic subsidence. Above 4500 m MSL θ increased less than 1 K. This corresponds to a downward motion of ~200 m within 12 h if the warming was only caused by adiabatic subsidence. In addition, the top of the observed elevated layer (~4000 m MSL) agrees well with observations from case studies within the Alps (Nyeki et al. 2000; Carnuth and Trickl 2000; Henne et al. 2004). Therefore, the assumption that an air parcel stays at about the same height during the advection process is justified.

For the same criteria and daytime advection average relative humidities (not shown) were lower than 40% on the windward side and between 50% and 60% on the lee side. This underlines that if condensation occurred it was only very localized. Clouds dissolved before they reached the sounding site in Milan.

Radiosondes with different humidity sensors were used at the two sounding sites. In general, the accuracy of humidity sensors of radiosondes is lower for low temperatures. Differences between the two stations might result from this lack of accuracy for individual soundings. No systematic difference could be observed for average specific humidities in an air mass that was advected from Payerne to Milan in situations without considerable vertical exchange (nighttime, Fig. 9 and above 4500 m MSL for all other no-lightning categories).

Because of humidity sensor changes at the Swiss sounding site in 1992 and 2001, calculations were carried out for two separate periods (1991 + 2001 + 2002, and 1992–2000). The general structure of the findings for the SND_{nl} and RAD_{nl} case did not change from the first period to the second. But specific humidity was larger in the first period than in the second, especially in the 0000 UTC Milan sounding, resulting in a somewhat larger increase in specific humidity in the first period. Whether this is due to the instrument changes or climatological variation could not be determined by this study.

Instead of using lightning measurements taken at surface stations between Payerne and Milan, the convective available potential energy (CAPE) was estimated from the 1200 UTC soundings at both sites to partition between days with and without deep convection. The results for the low CAPE (<2500 J kg^{-1}) and the no-lightning categories are similar. The same is true for the high CAPE (>2500 J kg^{-1}) and lightning categories. The median CAPE for SND_{nl} and RAD_{nl} were 1300 and 1600 J kg^{-1}, respectively, while for the lightning categories (SND_l and RAD_l) the median CAPE was much larger (2900 and 2900 J kg^{-1}, respectively). Therefore, CAPE can be used in situations where no lightning measurements are available to distinguish between days with or without potential for deep convection.

d. Dependence on atmospheric parameters

This subsection addresses the question of whether it is possible to find a relationship between the export rate f_e and atmospheric parameters like the total solar radiation per day ΣR_s, ff, or static stability $d\theta/dz$. For this analysis the whole dataset (12 yr) was selected. Days with lightning or rain were still excluded. The export rate f_e was rather independent of height within the altitude range of 2500–3500 m MSL (IL). For days with advection from Payerne at 1200 UTC toward Milan at 0000 UTC the average f_e in the IL was estimated. In contrast to f_e, f_t could not be calculated for individual days, because the direct advection was not detected at all altitudes above 2500 m MSL. In addition to f_e, different atmospheric parameters were derived for each individual day: ΣR_s, ΣS, q_{abl} from stations in the Alpine boundary layer below 1500 m MSL; $\mathrm{ff}_{\mathrm{il}}$, T_{il}, $q_{a,\mathrm{il}}$ from radio soundings within the IL; $d\theta/dz$, $d\theta_e/dz$, $d\theta/dz_{\max}$ from radio soundings from the surface up to 5000 m MSL.

The highest correlation of f_e with any of the other parameters was determined for ΣR_s: $r = 0.41$. The correlation with ΣS and q_{abl} was 0.37 and 0.35, respectively. The latter is remarkable, because f_e is a quantity that was already normalized by q_{abl}. Larger specific humidity within the ABL might cause condensation when air is transported upward and, therefore, assists in vertical motion and ABL air export. Only a weak correlation was observed for the specific humidity in the IL on the windward side $q_{a,\mathrm{il}}$ ($r = -0.14$). The wind speed in the IL and f_e were not correlated ($r = -0.03$), supporting the residence time concept presented in section 2. Of the stability parameters $d\theta/dz$ showed the most negative correlation: $r = -0.33$.

Correlations of average ri within the IL with the specified atmospheric parameters showed generally lower absolute values for all parameters with the exception of wind speed $\mathrm{ff}_{\mathrm{il}}$ ($r = -0.16$).

Figure 12 shows a box plot of average f_e within the IL for different categories of ΣR_s. The fraction of ABL air that was injected into a layer of 100-m thickness per hour is f_e. Multiplying f_e by 10 gives the fraction of ABL air that was injected into the IL (1000 m thickness) per hour. There is a considerable trend of larger median f_e for larger ΣR_s. Also visible is the large spread of the data within the different categories. Some outliers also influenced the mean (stars) of the category, increasing the trend for the mean relative to the median. Days with ΣR_s lower than 7.5 MJ m^{-2} showed a negative median of f_e. Subsidence was dominating on these days. Days with R_s larger than 12.5 MJ m^{-2} favored positive ABL export over the Alpine terrain between Payerne and Milan.

Figure 13 shows a box plot of average f_e within the IL for different categories of $d\theta/dz$. In general, there was a trend to larger f_e for lower stabilities (lower $d\theta/dz$). But, median and mean f_e showed maximal values for $d\theta/dz$ in the range of 3–4 K km^{-1} and lower values for $d\theta/dz = 2$ K km^{-1}. More cases with low stability would be necessary to prove this tendency. For large atmospheric stability ($d\theta/dz > 5$ K km^{-1}) negative values of f_e dominated in these situations. Vertical transport was too weak to counteract the strong atmospheric stability. Too few cases with very strong atmospheric stability ($d\theta/dz = 7$–8 K km^{-1}) were included in the analysis to determine if the mean and median for f_e were only due to some extreme events.

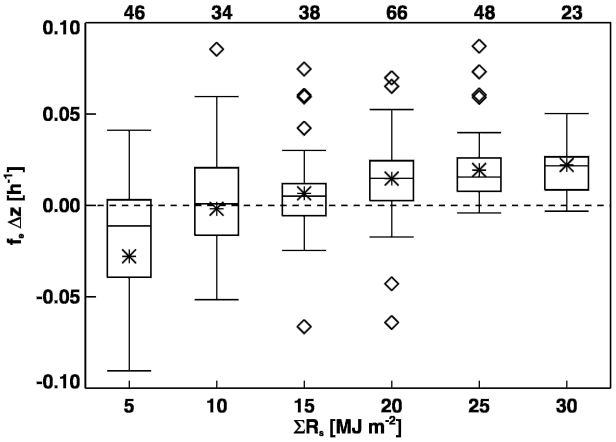

FIG. 12. Box plot of average ABL export rate $f_e\Delta z$ in the altitude range from 2500 to 3500 m MSL for different categories of total global radiation ΣR_s. Mean values for each category are displayed as stars. Outliers are indicated with diamonds. The number of cases in each category is displayed above the plot area.

4. Conclusions

Elevated layers of increased moisture were observed in average vertical profiles within an altitude range from 2500 to 4000 m MSL on fair-weather days (se-

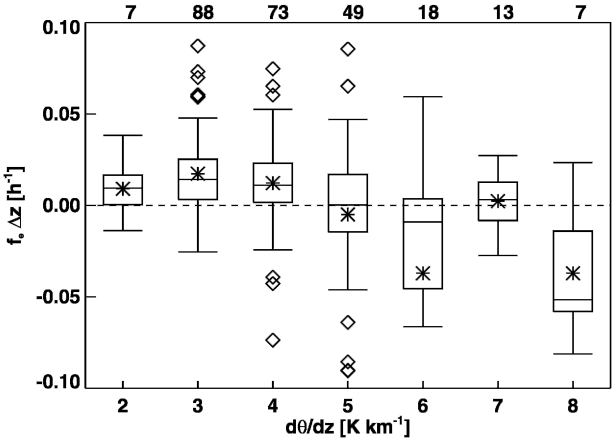

FIG. 13. Same as Fig. 12, but for different categories of potential temperature gradient $d\theta/dz$ between the surface and 5000 m MSL.

lected by different criteria SND, RAD, ANT, and IND) for air that was advected from Payerne at 1200 UTC toward Milan at 0000 UTC. This increase in the leeside sample was also apparent for all of JJA. If this increase would be caused by a dynamic process (e.g., mountain waves) one should also observe a similar picture for nighttime advection. Because no leeside nighttime increase of specific humidity could be observed, we conclude that the leeside daytime increase has to be attributed to upward motion in daytime thermally driven flow systems in the Alps (mountain venting).

All of the observed elevated layers were well above the observed daytime ABL heights at Payerne and Milan. Transport of elevated layers out of the mountainous region consequently leads to export of ABL air to the FT. Therefore, mountain venting under fair-weather daytime conditions increases vertical ABL export in comparison with flat terrain.

The characteristics of elevated layers agree well for different criteria to select fair-weather days, based on surface observations (SND, RAD) and Alpine Weather Statistic (AWS) (ANT, IND). Hence, AWS is a good tool to identify fair-weather days during the summer half-year.

The results of the layer method agree with the results of the profile method. Potential temperature increased only slightly from the windward to the lee side, showing that the altitude of an air parcel after mountain passage was relatively unaltered. Average relative humidity stayed below 60%, ensuring that only minor condensation occurred during the transport. Therefore, the described method was found to be suitable for the investigation of vertical export processes over mountainous terrain.

The upper bound of the elevated moisture layer corresponds well with the aerosol-layer height observed by backscatter lidar and q profile measurements in the central Alps (Henne et al. 2004; Nyeki et al. 2000; Carnuth and Trickl 2000). All of these measurements took place within the Alps between Payerne and Milan on fair-weather days. Together with observations of volatile organic compounds (Prevot et al. 2000), the lidar measurements suggest that not only is moisture lifted over the Alpine terrain and transported horizontally toward the plains, but so too are aerosols and other ABL pollutants.

The average fraction of ABL air within the elevated layers was as large as 0.24–0.33 for advection from Payerne toward Milan within the SND, RAD, ANT, CYC, and JJA no-lightning categories. Prevot et al. (2000) quantified the relative increase ri for different volatile organic compounds and specific humidity at 3000 m MSL above the Mesolcina valley in southern Switzerland. Here ri was observed in the range of 15%–45%, which compares well to our observations for ri for specific humidity.

The fractional export rate from the ABL was calculated to be 0.25–0.32 h^{-1} for the same categories as before, that is, 25%–32% of the ABL air mass was exported to the FT per hour. Locally, the ABL exchange rate was estimated by using mass budgets to be 0.28–0.42 h^{-1} on eight different days for two different valleys in southern Switzerland (Henne et al. 2004). The results of our climatological analysis agree with their findings.

The good agreement for ri and f_e for our climatological study and the local studies also implies that the locally observed export rates are representative for a larger area in the Alps, at least the catchment area for the Milan soundings.

About 220 days out of the investigation period of 12 yr showed advection from Payerne toward Milan and fulfilled the SND, RAD, ANT, or IND criterion. The criteria itself selected 540, 918, 416, and 796 days, respectively. Vertical export also takes place on these days but was not detectable with the setup of this study. Elevated layers are likely to be formed on about 50%–60% of all days during the summer season, potentially influencing lower-tropospheric air pollutant budgets considerably. Trajectory analysis shows that the Mediterranean and North Africa are potentially influenced by pollutants that are lifted above Alpine terrain (Henne et al. 2004).

The chemical composition and ozone production within the elevated layers will be analyzed in the future by using a chemical box model for case and climatological studies. Further intensive field campaigns on an Alpine scale should be performed to gather more information about the chemical composition and horizontal length of the elevated layers. Because specific humidity is not a totally conservative quantity, analyses similar to our study but that consider other parameters are desirable. The aerosol backscatter that is measured by lidar could be one promising parameter because of its high vertical resolution and the already existing measurement network.

Acknowledgments. We thank MeteoSwiss, and especially Pierre Jeannet, for providing the radio soundings and surface data that were used in this study.

REFERENCES

Alexandris, S., and P. Kerkides, 2003: New empirical formula for hourly estimations of reference evapotranspiration. *Agric. Water Manage.,* **60,** 157–180.

Baltensperger, U., H. W. Gaggeler, D. T. Jost, M. Lugauer, M. Schwikowski, E. Weingartner, and P. Seibert, 1997: Aerosol climatology at the high-alpine site Jungfraujoch, Switzerland. *J. Geophys. Res.,* **102** (D16), 19 707–19 715.

Carnuth, W., and T. Trickl, 2000: Transport studies with the IFU three-wavelength aerosol lidar during the VOTALP Mesolcina experiment. *Atmos. Environ.,* **34,** 1425–1434.

Dai, A., J. H. Wang, R. Ware, and T. van Hove, 2002: Diurnal variation in water vapor over North America and its implications for sampling errors in radiosonde humidity. *J. Geophys. Res.,* **107,** 4090, doi:10.1029/2001JD000642.

De Wekker, S. F. J., D. G. Steyn, and S. Nyeki, 2004: A comparison of aerosol layer- and convective boundary layer structure

over a mountain range during STAAARTE '97. *Bound.-Layer Meteor.,* **113,** 249–271.
Durran, D. R., 1990: Mountain waves and downslope winds. *Atmospheric Processes over Complex Terrain, Meteor. Monogr.*, No. 45, Amer. Meteor. Soc., 59–81.
Forrer, J., R. Ruttimann, D. Schneiter, A. Fischer, B. Buchmann, and P. Hofer, 2000: Variability of trace gases at the high-Alpine site Jungfraujoch caused by meteorological transport processes. *J. Geophys. Res.,* **105** (D10), 12 241–12 251.
Furger, M., and Coauthors, 2000: The VOTALP Mesolcina Valley Campaign 1996—Concept, background and some highlights. *Atmos. Environ.,* **34,** 1395–1412.
Haberli, C. H., 2002: The Comprehensive Alpine Radiosonde Data Set. University of Vienna Tech. Rep., 68 pp. [Available online at http://homepage.univie.ac.at/christian.haeberli/techdocu.htm.]
Henne, S., and Coauthors, 2004: Quantification of topographic venting of boundary layer air to the free troposphere. *Atmos. Chem. Phys.,* **4,** 497–509.
Iwasaki, H., and T. Miki, 2001: Observational study on the diurnal variation in precipitable water associated with the thermally induced local circulation over the "semi-basin" around Maebashi using GPS data. *J. Meteor. Soc. Japan,* **79,** 1077–1091.
Kossmann, M., U. Corsmeier, S. De Wekker, F. Fiedler, R. Vögtlin, N. Kalthoff, H. Güsten, and B. Neininger, 1999: Observations of handover processes between the atmospheric boundary layer and the free troposphere over mountainous terrain. *Contrib. Atmos. Phys.,* **72,** 329–350.
Kuwagata, T., A. Numaguti, and N. Endo, 2001: Diurnal variation of water vapor over the central Tibetan Plateau during summer. *J. Meteor. Soc. Japan,* **79,** 401–418.
Lugauer, M., and P. Winkler, 2005: Climatology of the thermal circulation in the Alpine region in southern Bavaria. *Meteor. Z.,* **14,** 15–30.
——, U. Baltensperger, M. Furger, H. W. Gaggeler, D. T. Jost, M. Schwikowski, and H. Wanner, 1998: Aerosol transport to the high Alpine sites Jungfraujoch (3454 m ASL) and Colle Gnifetti (4452 m ASL). *Tellus,* **50B,** 76–92.
Mann, H. B., and D. R. Whitney, 1947: On a test of whether one of 2 random variables is stochastically larger than the other. *Ann. Math. Stat.,* **18,** 50–60.
Mendonca, B. G., 1969: Local wind circulation on the slopes of Mauna Loa. *J. Appl. Meteor.,* **8,** 533–541.
Nyeki, S., and Coauthors, 2000: Convective boundary layer evolution to 4 km ASL over high-alpine terrain: Airborne lidar observations in the Alps. *Geophys. Res. Lett.,* **27,** 689–692.
——, and ——, 2002: Airborne lidar and in-situ aerosol observations of an elevated layer, leeward of the European Alps and Apennines. *Geophys. Res. Lett.,* **29,** 1852, doi:10/1029/2002GL014897.
Ohtani, R., 2001: Detection of water vapor variations driven by thermally-induced local circulations using the Japanese continuous GPS array. *Geophys. Res. Lett.,* **28,** 151–154.
Prevot, A. S. H., J. Dommen, and M. Baeumle, 2000: Influence of road traffic on volatile organic compound concentrations in and above a deep Alpine valley. *Atmos. Environ.,* **34,** 4719–4726.
Rocken, C., T. Vanhove, J. Johnson, F. Solheim, R. Ware, M. Bevis, S. Chiswell, and S. Businger, 1995: GPS/STORM—GPS sensing of atmospheric water vapor for meteorology. *J. Atmos. Oceanic Technol.,* **12,** 468–478.
Sasaki, T., P. Wu, S. Mori, J. I. Hamada, Y. I. Tauhid, and M. D. Yamanaka, 2004: Vertical moisture transport above the mixed layer around the mountains in western Sumatra. *Geophys. Res. Lett.,* **31,** L08106, doi:10.1029/2004GL019730.
Schuepp, M., 1979: Witterungsklimatologie der Schweiz, Band III, Beilage zu den Annalen 1978. (Weather climatology of Switzerland. Vol. III: Supplement to the 1978 annals). Swiss Meteorological Institute Rep., 94 pp. [Available from Swiss Meteorological Institute, Krähbühlstrasse 58, Postfach 514, CH-8044 Zurich, Switzerland.]
Seibert, P., H. Kromp-Kolb, A. Kasper, M. Kalina, H. Puxbaum, D. T. Jost, M. Schwikowski, and U. Baltensperger, 1998: Transport of polluted boundary layer air from the Po Valley to high-alpine sites. *Atmos. Environ.,* **32,** 3953–3965.
——, F. Beyrich, S. E. Gryning, S. Joffre, A. Rasmussen, and P. Tercier, 2000: Review and intercomparison of operational methods for the determination of the mixing height. *Atmos. Environ.,* **34,** 1001–1027.
Takagi, T., F. Kimura, and S. Kono, 2000: Diurnal variation of GPS precipitable water at Lhasa in premonsoon and monsoon periods. *J. Meteor. Soc. Japan,* **78,** 175–180.
Tregoning, P., R. Boers, D. O'Brien, and M. Hendy, 1998: Accuracy of absolute precipitable water vapor estimates from GPS observations. *J. Geophys. Res.,* **103** (D22), 28 701–28 710.
Wanner, H., E. Salvisberg, R. Rickli, and M. Schuepp, 1998: 50 years of Alpine Weather Statistics (AWS). *Meteor. Z.,* **7,** 99–111.
Whiteman, C. D., 2000: *Mountain Meteorology.* Oxford University Press, 355 pp.
——, and X. D. Bian, 1996: Solar semidiurnal tides in the troposphere: Detection by radar profilers. *Bull. Amer. Meteor. Soc.,* **77,** 529–542.
Wu, P. M., J. I. Hamada, S. Mori, Y. I. Tauhid, M. D. Yamanaka, and F. Kimura, 2003: Diurnal variation of precipitable water over a mountainous area of Sumatra Island. *J. Appl. Meteor.,* **42,** 1107–1115.
Zellweger, C., and Coauthors, 2000: Summertime NO_y speciation at the Jungfraujoch, 3580 m above sea level, Switzerland. *J. Geophys. Res.,* **105** (D5), 6655–6667.